ChemComm

Ratiometric temperature sensing with fluorescent thermochromic switches

Journal:	*ChemComm*
Manuscript ID	CC-COM-11-2018-009482.R1
Article Type:	Communication

ChemComm

COMMUNICATION

Ratiometric temperature sensing with fluorescent thermochromic switches

Received 28th November 2018,
Accepted #

DOI: 10.1039/#

rsc.li/chemcomm

Mercedes M. A. Mazza,[a] Francesca Cardano,[a,b,c] Janet Cusido,[a,d] James D. Baker,[a] Silvia Giordani[b,e,f] and Françisco M. Raymo*[,a]

The connection of fluorescent chromophores to switchable heterocycles translates into molecular probes with ratiometric response to temperature. The opening and closing of their heterocyclic component equilibrates two emissive species with resolved fluorescence. Their relative emission intensities change monotonically with temperature to enable the visualizaztion of thermal distributions at the microscale.

The ability to measure temperature with spatial resolution at the sub-micrometer level is crucial for the fundamental understanding of diverse cellular processes[1–3] and can have profound technological implications.[4,5] The requirement of physical contact between sample and sensor, however, prevents the miniaturization of conventional thermometry to this dimensional scale. These limitations are stimulating the development of alternative thermometric methods based on optical measurements.[6] In this context, the noninvasive character, ultrahigh sensitivity and fast response times of fluorescence, together with the inherent temperature dependence of the excitation dynamics of organic chromophores, are particularly convenient.[7] Indeed, remarkable examples of molecular and macromolecular systems capable of responding to temperature with fluorescence changes have been reported already.[8–12] In most instances, temperature affects the rates of the radiative and nonradiative deactivation of these chemical thermometers and, as a result, alters the intensity of their emission bands. Nonetheless, concentration effects and optical artifacts can influence significantly intensity measurements at a single wavelength.[13–15] In order to overcome these complications, distinct organic chromophores with resolved emission bands can be paired within thermosensitive macromolecular or supramolecular constructs to ensure ratiometric temperature response.[16–20] Temperature-induced geometrical changes of the scaffold holding the two components together generally affect their excitation dynamics and their relative emission intensities. Structural designs to engineer thermosensitive dual emission from a single chromophore could be a valuable alternative to these established methods. Indeed, they could provide the opportunity to avoid the relatively large dimensions of macromolecular backbones or supramolecular containers to enable the implementation of molecular-sized thermometers with ratiometric response.

Thermochromic compounds alter reversibly their ability to absorb visible light in response to temperature.[21] Generally, the interconversion of two isomers with resolved absorption bands is responsible for these effects. In principle, the two interconverting species could be engineered also to emit in distinct spectral regions. Under these conditions, a change in temperature would alter the relative intensities of the two resolved emissions and offer the opportunity to perform ratiometric measurements. These considerations suggested the possibility to explore the influence of temperature on the opening and closing of oxazine heterocycles. Indeed, our laboratories developed already halochromic and photochromic fluorophores based these reversible transformations.[22–24] Presumably, their structural design can be adapted to impose thermal response with dual fluorescence.

The ring-closed and -open isomers of **1** (**Cl** and **Op** in Fig. 1) interconvert with fast kinetics in acetonitrile at ambient temperature.[25] Specifically, variable temperature ^{1}H NMR spectroscopy and time-resolved absorption spectroscopy indicate the rate constants for ring-opening and -closing to be 7×10^2 and 5×10^{-6} s^{-1} respectively at 298 K. The coumarin chromophores of the two isomers emit in resolved spectral windows.[26] Specifically, the emission maximum shifts

[a] Laboratory for Molecular Photonics, Departments of Biology and Chemistry, University of Miami, Coral Gables, USA. E-mail: fraymo@miami.edu.
[b] Nano Carbon Materials, Istituto Italiano di Tecnologia, Turin, Italy
[c] Department of Chemistry and Industrial Chemistry, University of Genoa, Genoa, Italy
[d] Department of Natural and Social Sciences, Miami Dade College – InterAmerican Campus, Miami, USA
[e] Department of Chemistry, University of Turin, Torino, Italy
[f] School of Chemical Sciences, Dublin City University, Glasnevin, Ireland
† Electronic Supplementary Information (ESI) available: experimental procedures; spectroscopic data; DFT calculations. See DOI: 10.1039/#

bathochromically by *ca.* 200 nm with the opening of the 2*H*,4*H*-benzo[1,3]oxazine (oxazine) heterocycle. Indeed, only then can the coumarin chromophore extend its electronic conjugation over the resulting indolium cation. In principle, the ratio between the intensities of the two resolved emissions should change with temperature, if this physical parameter can affect the equilibrium between the two isomers. Should this be the case, then the spontaneous opening and closing of oxazine heterocycles might become a viable mechanism to design fluorescence sensors capable of responding ratiometrically to temperature. These considerations suggested the investigation of the temperature dependence of the equilibria between the ring-closed and -open isomers of four related molecular switches (**1–4** in Fig. 1). Compound **3Cl** incorporates a carbazole chromophore, in place of the coumarin component of **1Cl**, and was synthesized according to a literature procedure from our laboratories.[27] Compounds **2Cl** and **4Cl** have a 2*H*,3*H*,4*H*,5*H*-[1,3]oxazole (oxazolidine) heterocycle, instead of the oxazine ring of **1Cl** and **3Cl**, and were prepared in a single step from known precursors (Fig. S1).[‡,§,28]

The absorption spectra (Fig. 2) of **1–4** in acetonitrile at micromolar concentrations show the characteristic bands of the coumarin and carbazole chromophores associated with the ring-closed isomers. Specifically, the wavelength (λ_{Ab}) of the absorption maximum for the coumarin component of **1Cl** and **2Cl** is 412 nm.[25] Those for the pair of bands corresponding to the carbazole chromophore of **3Cl** and **4Cl** are 240 and 287 nm.[27] Comparison to the absorption spectra of appropriate model compounds (**8** and **9** in Fig. S3) indicates that the carbazole absorptions partially overlap those associated with the indole and 4-nitrophenoxy fragments.

The absorption spectra of model compounds (**10** and **11** in Fig. S3) with extended chromophoric platforms analogous to those of **1Op**–**4Op** suggest that the coumarin and carbazole fragments of the ring-open isomers should absorb in the visible region. Indeed, bands in this spectral window can be detected when either the total concentration of the pair of interconverting isomers is raised to the millimolar level (Fig. S4) or in the presence of water (Fig. 2). These observations indicate that the ring-closed isomer is significantly more stable than the ring-open one in acetonitrile for all systems and that water facilitates ring opening. The latter effect can be a consequence of the increase in solvent polarity with a concomitant stabilization of **1Op**–**4Op** and/or their protonation to form **1OpH**–**4OpH**. Density functional theory[29] (DFT) calculations, performed on model compound **8** (Figs. S12 and S13) with solvation models for either acetonitrile or water, suggest that the change in the dielectric constant of the medium has a negligible influence on the relative energies of the two isomers.[¶,30] Instead, the pKa values reported in the literature[31] for 4-nitrophenol (7.15) and ethanol (15.50) imply that the protonation of the ring-open isomer is essentially quantitative in the presence of water. Thus, the absorption bands observed at long wavelengths in a mixture of acetonitrile and water can be assigned to the extended chromophores of **1OpH**–**4OpH**.

The absorption spectra (Figs. 3 and S5–S7) of **1–4** in a mixture of acetonitrile and water display significant temperature dependence.[#] In all instances, the absorbance of the ring-closed isomer at short wavelengths increases and that of the protonated form at long wavelengths decreases with a raise in temperature. From the absorbance values at the maxima of these bands, the concentrations of **1Cl**–**4Cl** and **1OpH**–**4OpH** can be estimated at each temperature (*T*) to quantify the corresponding equilibrium constants (K_{Eq}). In turn, the enthalpic (ΔH) and entropic ($T\Delta S$) terms governing these equilibria can be evaluated from the slope and intercept respectively of logarithmic plots (Fig. S8) of K_{Eq} against the inverse of temperature. The resulting values are listed in Table S1. In all instances, $T\Delta S$ is significantly more negative that ΔH in agreement with the pronounced temperature dependence of the absorption spectra. Interestingly, the ΔH values of the

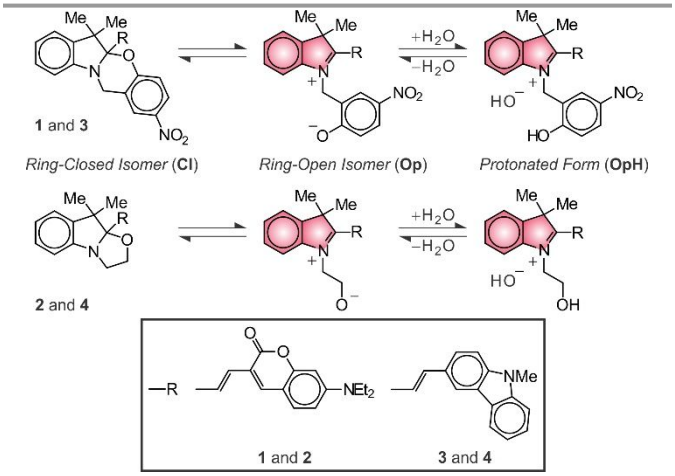

Fig. 1 Interconversion of the ring-closed (**Cl**) and -open (**Op**) isomers of **1–4** and their protonated forms (**OpH**).

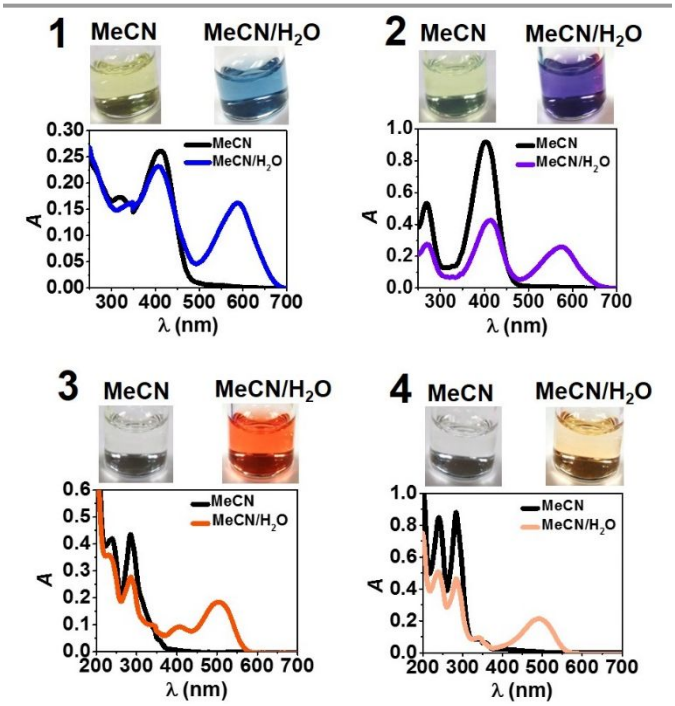

Fig. 2 Absorption spectra of **1–4** (15–120 μM) in MeCN and MeCN/H_2O (1:1 v/v) at 293 K and photos of the corresponding solutions.

oxazolidine derivatives (**2** and **4**) are more negative than those of the oxazine counterparts (**1** and **3**), consistently with the large pK_a difference between their protic functional groups. Similarly, the $T\Delta S$ values of the carbazole derivatives (**3** and **4**) are more negative than those of the coumarin counterparts (**1** and **2**), perhaps as a result of solvation effects and/or the conformational freedom associated with the diethylamino substituent of the latter.

In a mixture of acetonitrile and water, the coumarin chromophores of ring-closed isomers **1Cl** and **2Cl** absorb at a λ_{Ab} of 412 nm (Table S1) and produce fluorescence with emission maxima at wavelengths (λ_{Em}) of 475 and 489 nm respectively. However, the fluorescence quantum yield (ϕ) of **1Cl** is only 0.01, while that of **2Cl** is 0.98. Such a pronounced difference in ϕ indicates that the presence of a 4-nitrophenoxy fragment in **1Cl** must encourage the nonradiative deactivation of the excited coumarin fluorophore. A similar effect is observed also for protonated forms **1OpH** and **2OpH**. They emit at λ_{Em} of 650 and 660 nm with ϕ of 0.02 and 0.15 respectively. Once again, the presence of a 4-nitrophenol fragment in **1OpH** is promoting the nonradiative deactivation of the excited fluorophore. Presumably, the electron deficient nitro groups of **1Cl** and **1OpH** can accept an electron from the corresponding coumarin chromophores upon excitation in both instances to quench fluorescence.

Under the same experimental conditions, the carbazole chromophores of ring-closed isomers **3Cl** and **4Cl** absorb at λ_{Ab} of 240 and 287 nm (Table S1). However, only 4Cl produces fluorescence at λ_{Em} of 371 and 383 nm with ϕ of 0.18. The 4-nitrophenoxy fragment of **3Cl** must be responsible for suppressing the ability of the carbazole chromophore to emit. Indeed, literature data[27] from our laboratories suggest that the photoinduced transfer of one electron from the latter component to the former is exergonic with a free-energy change of –0.7 eV.[¥,32] Once again, a similar effect is observed also for protonated forms **3OpH** and **4OpH**. The extended electronic conjugation of their chromophoric platforms shifts λ_{Ab} to the visible region, but only the latter compound produces fluorescence at a λ_{Em} of 596 nm with ϕ of 0.02.

The significant temperature dependence of the equilibrium between the ring-closed isomer and protonated form of **1–4**, obvious from the absorption spectra, translates into a ratiometric fluorescence response. Indeed, the relative intensities of the emission bands of the two equilibrating species change with temperature (Figs. 3 and S5–S7) apart from **3**, which is essentially not emissive. This effect is especially evident for **2Cl** and **2OpH**, because their ϕ values are significantly larger than those of the other systems. Specifically, the emission band of **2Cl** at a λ_{Em} of 489 nm increases while that of **2OpH** at a λ_{Em} of 660 nm decreases with a raise in temperature. Plots (Figs. 3, S5 and S7) of the corresponding emission intensities against temperature show linear correlations in both instances with a monotonic increase in their ratio.

The ratiometric response of **2** can be exploited to probe temperature with spatial resolution at the micrometer level. Specifically, the resolved emissions of the two equilibrating species can be collected in separate detection channels of the same fluorescence microscope to allow ratiometric temperature measurements within microscaled regions of a given sample of interest. For example, **2** can be introduced within beads of alginate hydrogels. The presence of water in the beads encourages the partial conversion of **2Cl** into **2OpH** to establish an equilibrium between the two species. Consistently, emission spectra (Fig. S10) of a single bead suspended in water revel the resolved bands of the two emissive species. Once again, the band of **2Cl** increases and that of **2OpH** decreases with a raise in the temperature of the sample. No spectral changes (Fig. S11) are instead detected if the bead is maintained at a constant temperature, indicating

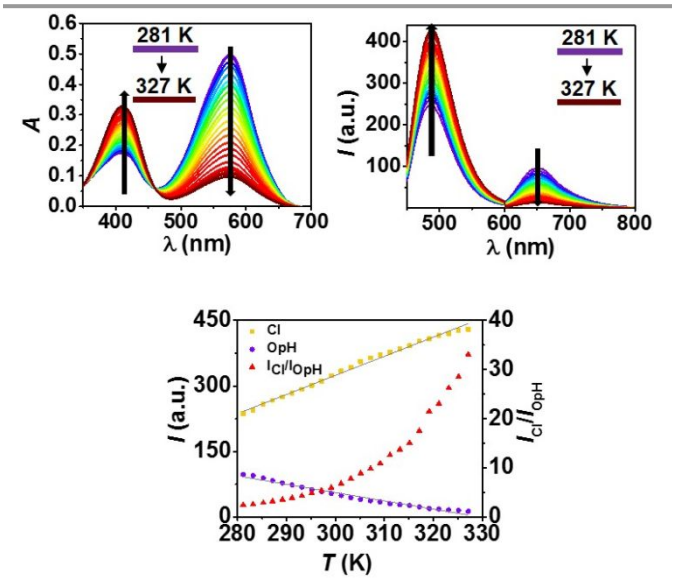

Fig. 3 Absorption (left) and emission (right, λ_{Ex} = 415 and 575 nm) spectra of **2** (24 μM) in MeCN/H_2O (1:1 v/v) at temperatures ranging from 281 to 327 K together with the temperature dependence (bottom) of the emission intensities of **Cl** and **OpH** and their ratio.

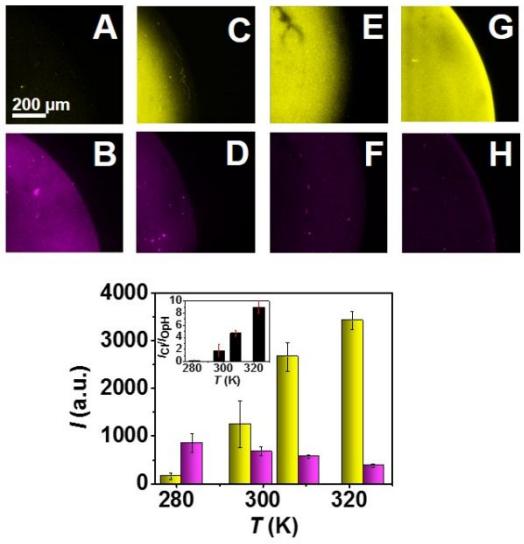

Fig. 4 Fluorescence images of an alginate bead (diameter = 1.6 mm), doped with **2** and maintained at 281 (**A** and **B**), 297 (**C** and **D**), 308 (**E** and **F**) or 323 K (**G** and **H**) together with the corresponding emission intensities, integrated across the field of view, and their ratio (inset) [Yellow Channel: λ_{Ex} = 405 nm, λ_{Em} = 450–600 nm; Purple Channel: λ_{Ex} = 561 nm, λ_{Em} = 600–770 nm].

that the two interconverting species are stable under these conditions. Images (**A**, **C**, **E** and **G** in Fig. 4) of the bead, recorded by collecting fluorescence between 450 and 600 nm where only **2Cl** emits, show an increase in emission intensity with temperature. Images (**B**, **D**, **F** and **H** in Fig. 4) of the very same sample, acquired with a detection window ranging from 600 to 770 nm where only **2OpH** emits, reveal a concomitant fluorescence decrease. Indeed, the ratio (black bars in Fig. 4) between the emission intensities (yellow and purple bars in Fig. 4), integrated across the fields of view of the two channels, clearly increases with the temperature of the sample.

In summary, the equilibration of two interconverting species with resolved fluorescence results in a ratiometric response to temperature. The opening and closing of either an oxazine or an oxazolidine heterocycle are responsible for this behavior. Indeed, these structural changes affect the electronic structure of either a carbazole or a coumarin fluorophore and control the spectral position of its absorption and emission bands. In turn, the resolved emissions of the two interconverting species can be probed in parallel spectroscopically as well as measured in independent detection channels of a single microscope. In both instances, the ratio between the detected intensities can be exploited to overcome concentration effects and optical artifacts, which complicate conventional single-wavelength measurements instead. In fact, this structural design for ratiometric sensing allows the convenient mapping of temperature distributions in microscaled samples with the acquisition of conventional fluorescence images.

The National Science Foundation (CHE-1505885) is acknowledged for financial support.

Conflicts of interest

There are no conflicts to declare.

Notes and references

‡ For a literature precedent on the synthesis of **2Cl**, see ref. 28.
§ ^{1}H NMR spectra (Fig. S2) of **2** in CD_3CN show significant broadening for the resonances associated with the two pairs of diastereotopic ethylene protons. These observations are indicative of the opening and closing of the oxazolidine ring with fast kinetics on the NMR timescale, consistently with the behavior reported previously for **1** (ref. 25).
¶ The free-energy barriers for ring opening ($\Delta G^{\ddagger}_{Op}$) and closing ($\Delta G^{\ddagger}_{Cl}$) and the free-energy difference (ΔG^0) between ring-open and -closed isomers, calculated in acetonitrile at 298 K, are 14.09, 5.85 and 8.23 kcal mol^{-1} respectively (ref. 30). The values of $\Delta G^{\ddagger}_{Op}$, $\Delta G^{\ddagger}_{Cl}$ and ΔG^0 estimated in water at the same temperature are 13.95, 6.20 and 7.76 kcal mol^{-1} respectively (Fig. S13).
# Similar results (Fig. S9) are observed in mixtures of MeCN and H_2O with relative amounts of the two solvents ranging from 4:1 to 1:1 (v/v). Aggregation occurs upon further increase of the H_2O content.
¥ The free-energy change (ΔG^0_{ET}) for the photoinduced electron transfer process was calculated with eq. 1 (ref. 32). The oxidation (E_{Ox}) and reduction (E_{Red}) potentials as well as the optical band-gap energy (ΔE_{Op}) of appropriate model compounds are reported in ref. 27. The donor–acceptor distance (d) was estimated to be 11 Å.

$$\Delta G^0_{ET} = eE_{Ox} - eE_{Red} - \Delta E_{Op} - \frac{e^2}{4\pi\varepsilon_0\varepsilon_r d} \quad (1)$$

1 J. Qiao, X. Y. Mu and L. Qi, *Biosens. Bioelectr.*, 2016, **85**, 403–413.
2 T. T. Bai and N. Gu, *Small*, 2016, **12**, 4590–4610.
3 S. Uchiyama, C. Gota, T. Tsuji and N. Inada, *Chem. Commun.*, 2017, **53**, 10976–10992.
4 H. Y. Zhou, M. Sharma, O. Berezin, D. Zuckerman and M. Y. Berezin, *ChemPhysChem*, 2016, **17**, 27–36.
5 B. del Rosal, E. Ximendes, U. Rocha and D. Jaque, *Adv. Opt. Mater.*, 2017, **5**, 1600508-1–14.
6 M. Quintanilla and L. M. Liz-Marzan, *Nano Today*, 2018, **19**, 126–145.
7 J. R. Lakowicz, *Principles of Fluorescence Spectroscopy*, Springer, New York, 2006.
8 S. Uchiyama, A. P. de Silva and K. Iwai, *J. Chem. Ed.*, 2006, **83**, 720–727.
9 C. Pietsch, U. S. Schubert and R. Hoogenboom, *Chem. Commun.*, 2011, **47**, 8750–8765.
10 X.-D. Wang, O. S. Wolfbeis and R. J. Meier, *Chem. Soc. Rev.*, 2013, **42**, 7834–7869.
11 J. Rocha, C. D. S. Brites and L. D. Carlos, *Chem. A Eur. J.*, 2016, **22**, 14782–14795.
12 T. Y. Qin, B. Liu, K. N. Zhu, Z. J. Luo, Y. Y. Huang, C. J. Pan and L. Wang, *Trac-Trends Anal. Chem.*, 2018, **102**, 259–271.
13 E. J. McLaurin, L. R. Bradshaw and D. R. Gamelin, *Chem. Mater.*, 2013, **25**, 1283–1292.
14 S. Uchiyama and C. Gota, *Rev. Anal. Chem.*, 2017, **36**, 20160021.
15 Y. Cheng, Y. Gao, H. Lin, F. Huang and Y. S. Wang, *J. Mater. Chem. C*, 2018, **6**, 7462–7478.
16 T. Barilero, T. Le Saux, C. Gosse and L. Jullien, *Anal. Chem.*, 2009, **81**, 7988–8000.
17 X. D. Wang, X. H. Song, C. Y. He, C. J. Yang, G. Chen and X. Chen, *Anal. Chem.*, 2011, **83**, 2434–2347.
18 T. Liu and S. Y. Liu, *Anal. Chem.*, 2011, **83**, 2775–2785.
19 T. Kan, H. Aoki, N. Binh-Khiem, K. Matsumoto and I. Shimoyama, *Sensors*, 2013, **13**, 4138–4145.
20 J. Liu, X. Guo, R. Hu, J. Xu, S. Wang, S. Li, Y. Li and G. Yang, *Anal. Chem.*, 2015, **87**, 3694–3698.
21 J. C. Crano and R. Guglielmetti (Eds.), *Organic Photochromic and Thermochromic Compounds*, Plenum Press, New York, 1999.
22 M. Tomasulo, S. Sortino and F. M. Raymo, *J. Photochem. Photobiol. A*, 2008, **200**, 44–49.
23 E. Deniz, M. Tomasulo, J. Cusido, S. Sortino and F. M. Raymo, *Langmuir*, 2011, **27**, 11773–11783.
24 Y. Zhang, S. Tang, E. R. Thapaliya, L. Sansalone and F. M. Raymo, *Chem. Commun.*, 2018, **54**, 8799–8809.
25 E. Deniz, M. Tomasulo, J. Cusido, I. Yildiz, M. Petriella, M. L. Bossi, S. Sortino and F. M. Raymo, *J. Phys. Chem. C*, 2012, **116**, 6058−6068.
26 J. Cusido, S. Shaban Ragab, E. R. Thapaliya, S. Swaminathan, J. Garcia-Amorós, M. J. Roberti, B. Araoz, M. M. A. Mazza, S. Yamazaki, A. M. Scott, F. M. Raymo and M. L. Bossi, *J. Phys. Chem. C*, 2016, **120**, 12860–12870.
27 J. Garcia-Amorós, S. Swaminathan, S. Sortino and F. M. Raymo, *Chem. Eur. J.*, 2014, **20**, 10276–10284.
28 Q. H. You, Y. M. Lee, W. H. Chan, N. K. Mak, A. W. Lee, S. C. Hau and T. C. Mak, *RSC Adv.*, 2015, **5**, 4099–4102.
29 R. G. Parr and W. Yang, *Density-Functional Theory of Atoms and Molecules*, Oxford University Press, Oxford, 1989.
30 F. M. Raymo, *J. Phys. Chem. A*, 2012, **116**, 11888–11895.
31 D. R. Lide, *CRC Handbook of Chemistry and Physics*, CRC Press, Boca Raton, 2011.
32 G. J. Kavarnos, *Fundamentals of Photoinduced Electron Transfer*, VCH, New York, 1993.

Graphic for the Table of Contents